ELSEVIER

Journal of Nuclear Materials 290–293 (2001) 882–886

journal of nuclear materials

www.elsevier.nl/locate/jnucmat

Island divertor investigations on the W7-AS stellarator

R.W.T. König *, K. McCormick, Y. Feng, S. Fiedler, P. Grigull, D. Hildebrandt, J. Kisslinger, J.P. Knauer, G. Kühner, D. Naujoks, J. Sallander, S. Sardei, F. Wagner, A. Werner, W7-AS Team

Max-Planck-Institut für Plasmaphysik, EURATOM Association, MPI, Boltzmannstr. 2, 85748 Garching, Germany

Abstract

The effectiveness of 10 newly installed control coils, which had already been implemented in preparation for the upcoming divertor experiments, has been demonstrated in several important areas. Most importantly we have been able to show that the control coils can be used to influence the ratio of parallel to cross-field transport within an island by nearly a factor 2. High recycling conditions have been attained at the inboard limiters for $\iota(a) = 5/9$ but there was no indication of detachment. Excellent data consistency has been achieved during the high density phase of the high recycling discharges between the saturation current I_{sat} measured by the target Langmuir probes and the equivalent values derived from the new absolutely calibrated signal of the 2D H_α CCD camera. Poloidal as well as toroidal asymmetries caused considerable problems when we tried to relate measurements of different edge/target diagnostic signals, taken at equivalent positions around the machine. These asymmetries could with high probability be attributed to toroidally non-symmetrically distributed components like the diamagnetic loop (module 5) or the MINISOX camera (module 3).

Keywords: Plasma–material interaction; Hydrogen; Hydrides

1. Introduction

The suitability of the island divertor concept for the next generation of stellarators, and here in particular for W7-X, will be tested in detail on W7-AS in the coming experimental campaign. A set of 10 discrete divertor modules, similar to those proposed for W7-X, are presently being installed on W7-AS.

In preparation for this exercise a set of 10 control coils has already been installed in the machine, giving ample control on critical aspects of the island geometry. This already allowed us to perform some preliminary studies of the edge and scrape-off layer (SOL), albeit still with a set of 10 inboard sector limiters. The 5/9 boundary island configuration has got the most favourable geometry for inboard limiter as well as divertor module operation. This configuration has been chosen as a good compromise between large island size (~5 cm radially and poloidally in the triangular plane) at a still reasonable effective plasma radius ($a_{eff} \sim 14$ cm).

In this paper we report on a number of experiments which were performed in order to verify the effect of the control coils and on our efforts to document the edge plasma parameters under high recycling conditions with an enlarged set of edge diagnostics in order to build up a reference data set for the coming divertor experiments.

2. New edge diagnostics

A number of new edge diagnostics became available during the last experimental campaign. A new edge dedicated Thomson scattering system [1] allows one to measure n_e and T_e with a spatial resolution of 4 mm over a range of 120 mm at the high field side in the triangular plane of module 1 once per pulse. An interference filter based H_α imaging system with a spatial resolution of 0.5 mm equipped with a 2D CCD camera with a dynamic range of 12 bit has also been newly installed on W7-AS

* Corresponding author. Tel.: +49-89 3299 1219; fax: +49-89 3299 2584.

E-mail address: ralf.koenig@ipp.mpg.de (R.W.T. König).

0022-3115/01/$ - see front matter
PII: S0022-3115(00)00540-7

as a first step of a more comprehensive filter based imaging system [2]. This system allows one to monitor the H_α radiation distribution across the entire upper inboard limiter of module 5 with a temporal resolution of typically 20 ms. An In-Sb IR camera allowed one to determine the heat flux distribution across the upper inboard limiter of module 1 via a 3D finite element program with a spatial resolution of 3mm and a time resolution of 20 ms [3]. This system was complemented by already existing thermocouples for each individual tile of the upper and lower inboard limiters of modules 1 and 3, which allowed to investigate poloidal and toroidal asymmetries. A set of 8 flash mounted Langmuir probes was installed in both the upper and the lower inboard limiter of module 2. The probes had a poloidal separation of 30 mm and were swept at 500 Hz.

3. Control coil related experiments

3.1. Variation of the plasma radius via the control coils

First tests with the newly installed control coils have proven their ability to influence the plasma edge. The capability to vary the plasma radius via the control coils is clearly visible in the radial electron temperature profiles (plotted as a function of frequency) measured by the ECE diagnostic (Fig. 1). Moreover vacuum field predictions of effective plasma radius changes as a function of the control coil currents have been roughly validated via the $W_{dia} \sim a_{eff}^2$ scaling (Fig. 2).

3.2. Variation of the footprint location with I_{cc}

A further indication of the effectiveness of the control coils is the predicted and observed phase jump in the island structure for control coil currents $I_{cc} > 3$ kA (Fig. 3). At such high currents the field produced by the control coils exceeds the inherent field responsible for the islands thereby causing a poloidal exchange of the *x*- and *o*-points of the island structure. Experimentally this has been verified for $\iota_a = 1/2$ by a poloidal array of Langmuir probes operating in the shadow of the inboard limiters.

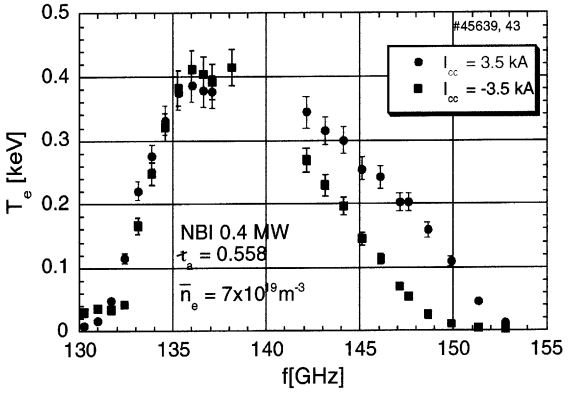

Fig. 1. Radial temperature profiles (here plotted versus frequency), measured with the ECE diagnostic, at the two extreme control coil currents.

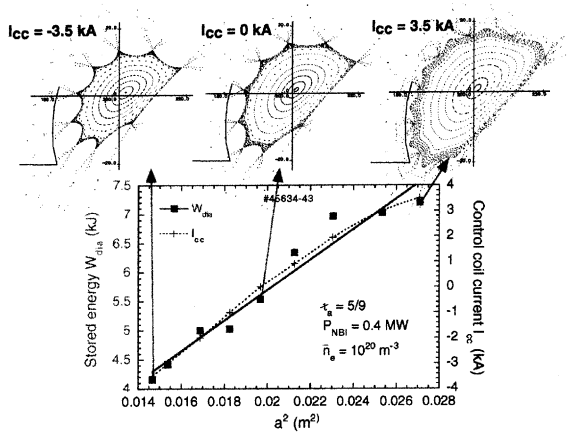

Fig. 2. W_{dia} and I_{cc} vs a_{eff}^2 at $\langle n_e \rangle = 1 \times 10^{20}$ m^{-3}. The plasma radius changes as expected from vacuum field calculations. A poloidal cross section through the field line structure is shown for three different control coil currents.

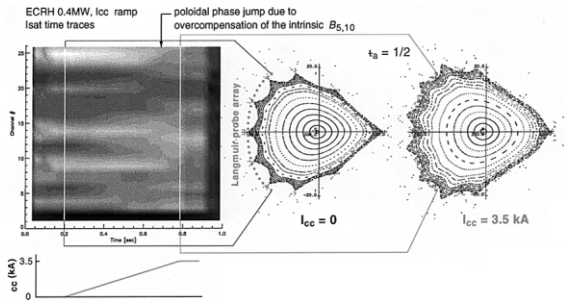

Fig. 3. Top: I_{sat} profile measured by the poloidal Langmuir probe array during a control coil current ramp (bottom).

3.3. Affecting the ratio of cross field to parallel transport via the control coils

If one assumes particle and momentum transport to be governed by parallel classical convection with a sound speed c_s and a perpendicular anomalous diffusion described by a diffusion coefficient D, then the parallel and perpendicular transport time scales can be roughly estimated as $\tau_{\|} = L_c/c_s$ and $\tau_{\perp} = 2r_i^2/D$ with r_i being the island radius, $L_c = R\pi/\Delta\iota_i$ being the field line connection length measured from the stagnation point to the

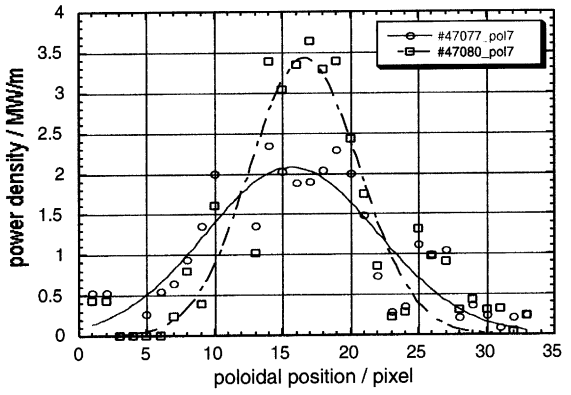

Fig. 4. Broadening of the power deposition profile with increasing connection length L_c. #47080: $L_c = 60$ m; #47077: $L_c = 110$ m.

target, and $\Delta\iota_i$ being the internal rotational transform within an island [4]. With the control coils it was possible to change the ratio of parallel to cross-field transport $\tau_{\|}/\tau_{\perp} \sim L_c/r_i^2$ by a factor of 1.8 by increasing the connection length L_c (averaged over the strike point region) from 60 to 110 m by reducing the control coil current from $I_{cc} = -3.5$ to 0 kA at a fixed X-point height of 3 cm above the inner limiters. The longer L_c did result as expected in a broadening of the power deposition profile derived from IR camera observations (Fig. 4) and a widening of the H_α emission profiles (Fig. 5) by a factor of 1.6 ± 0.1 and $\sim$1.3, respectively. Only the strike point located near the centre of the inner limiter could be used for this experiment since the field lines near the upper strike point were 'shadowed' by build-in components. This problem is specific to the inboard limiter case and will be absent with the new divertor modules.

4. Attainment of high-recycling conditions at the inboard limiters at $\iota(a) = 5/9$

A considerable part of our investigations was concentrated on the achievement of high recycling conditions near the inboard limiters [5,6]. The primary upstream goal for entering into a high recycling state near the target plates (here the limiters) is the attainment of high H-mode separatrix densities n_{es} at the lowest possible input power. Unfortunately with increasing density at constant input power one unavoidably gets into an ELM-free quiescent H-mode regime [7,8], which is incompatible with a high recycling divertor regime since it is always accompanied by low edge densities. Therefore high neutral beam heating power to get above the H-mode density threshold $\langle n_{e,thr} \rangle$ is required (Fig. 6), which leads to a further increase in n_{es}. Strong gas puffing is used as a further measure to increase the edge density.

With ECRH heating powers of 0.4 and 0.8 MW the density near the limiter n_{elim} follows n_{es} more or less linearly, i.e., one observes no sign of high recycling. At the limiter the densities n_{elim} remain below 1.5×10^{19} m^{-3}, while $T_{elim} = 25$–75 eV and $T_{es} = 80$–45 eV throughout the discharges. ECM3 calculations, not taking into account the effect of impurities, predict for the W7-AS divertor geometry high recycling conditions at $n_{es} \sim 4 \times 10^{19}$ m^{-3}. We explored the regime of very high values of n_{es} by going to $P_{NBI} = 2$ MW, thereby avoiding falling into the quiescent H-mode. Different gas puff rates exceeding the NBI fuelling rate by an order of magnitude were used. Transiently a maximum of $n_{es} = 9 \times 10^{19}$ m^{-3} at $T_{es} \sim 80$ eV was achieved with $n_{elim} > 1.5 \times 10^{20}$ m^{-3} at $T_{elim} < 10$ eV. At these conditions one would expect detachment to be imminent. However there are no indications for detachment (Fig. 7) since one does not observe a drop in power deposited

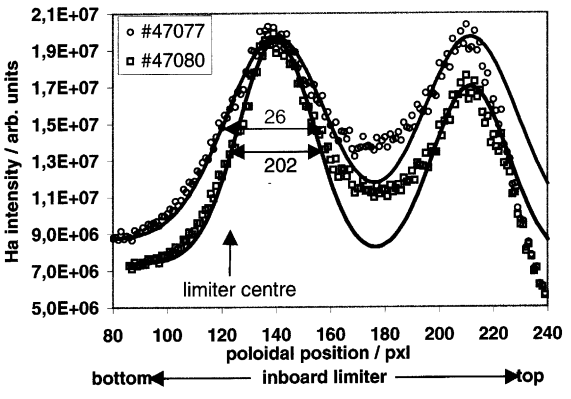

Fig. 5. Broadening of the H_α emission profile with increasing connection length L_c. #47080: $L_c = 60$ m; #47077: $L_c = 110$ m.

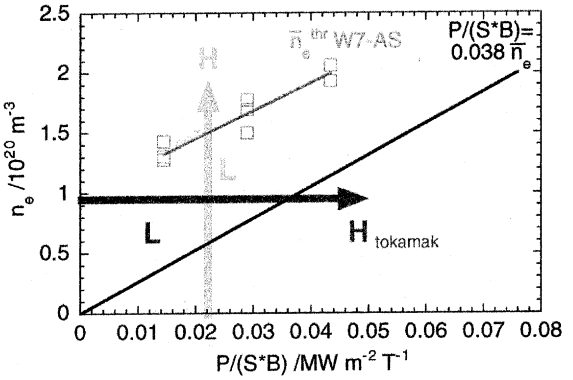

Fig. 6. The route into the H-mode in the W7-AS stellarator is orthogonal to the one in tokamaks [9]. P: heating power, S: plasma surface area, B: magnetic field.

on the upper limiter in module 1 with the IR camera. Also the saturation current I_{sat} measured by a Langmuir target probe at the main strike point on the bottom limiter in module 2 shows no drop (as one would expect at detachment). I_{sat} at the equivalent position on the top limiter of module 2 is about a factor 2 larger but unfortunately constrained by the power supply during high density phase. One also does not observe any strong increase in H_α radiation (as one would expect at detachment due to volume recombination). The I_{sat} values calculated from the H_α radiation measured at the probe position on the top limiter of module 5 are consistent with the probe measurements at the equivalent position at the bottom limiter in module 2 during the high density phase. During the low density phase $I_{sat}(H_\alpha)$ is about a factor of 2.5 lower than the Langmuir probe measurement. The reason for this is that during this phase the edge plasma is transparent for neutrals (long ionisation lengths) so that the plasma parameters derived from target probe measurements can no longer be used to calculate the number of ionisations per photon. The number of ionisations per photon were calculated using the ADAS package [10].

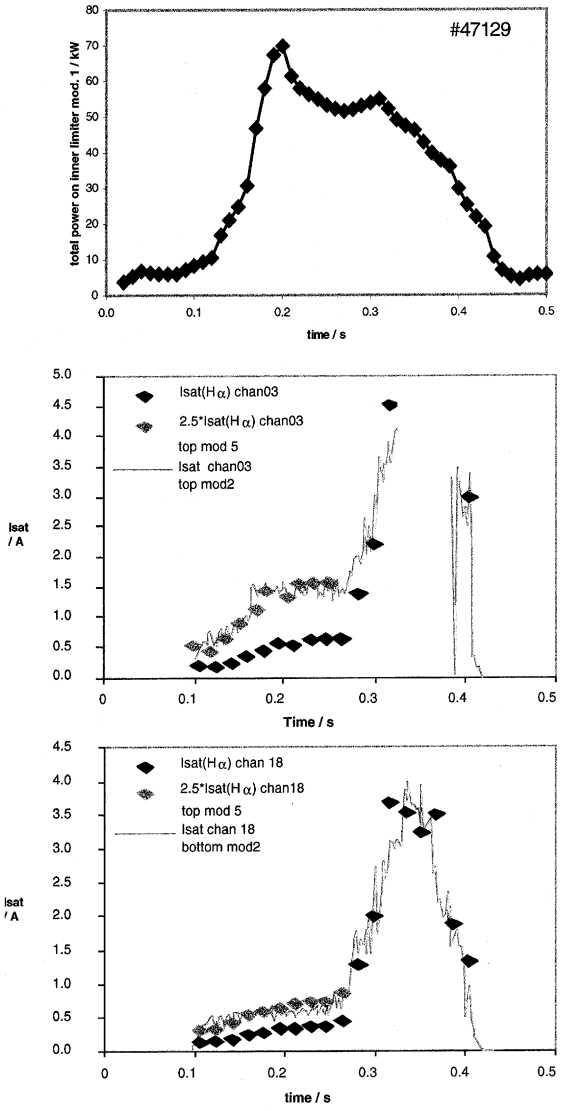

Fig. 7. Top: Total power on the upper inboard limiter in module 1; Centre and bottom: Comparison of I_{sat} measured by the target probes at the main strike point locations on the top (chan 03) and bottom (chan 18) inboard limiters in module 1 with I_{sat} calculated from the H_α emission at the equivalent target probe location on the top limiter in module 5.

5. Poloidal and toroidal asymmetries

A comparison of measurements from different diagnostics like Langmuir probes, IR and H_α camera and several calorimeters shows that we are severely affected by poloidal as well as toroidal asymmetries. These are at least partly caused by different degrees of shadowing of each individual inner limiter by components, which are not distributed symmetrically around the machine.

5.1. $E_r \times B$ drift in the island SOL

A considerable part of the up/down (poloidal) asymmetry, which reverses with a change of the magnetic field direction and gets smaller at higher densities, seems to be linked to an $E_r \times B$ drift within the island (Fig. 8), which has been observed before in low power, very low density discharges (like #47748 and #47755) but which one would not have expected to play a significant role at the high down-stream densities of the present high recycling experiments (e.g., pulse #47129 shown in Fig. 7). A quantitative assessment of the drift effects for high-density plasmas is beyond the present

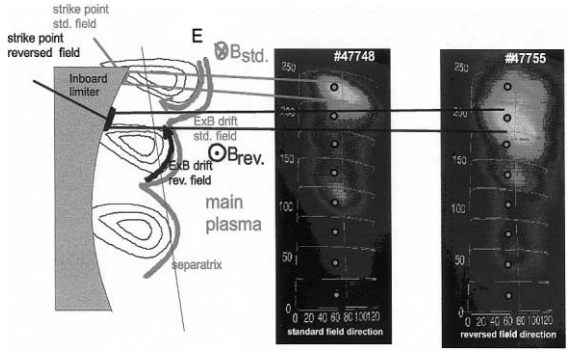

Fig. 8. Effect of the $E_r \times B$ drift on the strike point location for standard and reversed field operation for two very low density pulses. The green circles indicate the locations of the target integrated Langmuir probes.

capability of the ECM3 code (self-consistent 3D treatment of the drifts required) [11], i.e., an interpretation as E_rxB drift is not as obvious anymore in this parameter regime and consequences for operation with divertor modules are still open. For the divertor campaign particular efforts are undertaken to concentrate most edge diagnostics at one location in one module, accompanied by careful monitoring of any toroidal and poloidal asymmetries.

5.2. Poloidal asymmetries

Build-in non-symmetrically distributed mechanical components lead locally to a shortening of the field line connection lengths. In the example shown (Fig. 8) the main strike point is located near the top of the upper inner limiter (region of longest connection length). The overall field geometry is such that one should find the mirror image of the structure on the bottom limiter. However in the case of module 2 the diamagnetic loop leads to a quite considerable shielding of the main strike point on the bottom limiter. This effect could explain the observed discrepancy between I_{sat} measured by the top and bottom Langmuir probes, which are located exactly at these two locations, of about a factor 2.5 in a similar pulse (Fig. 7).

5.3. Toroidal asymmetries

Toroidally not symmetrically distributed components like the control coils, the diamagnetic loop, the Minisox camera cause locally a shortening of the magnetic field line connection lengths. Through this effect the interaction of the plasma with the target plates is, as observed by H_α, calorimetry and the IR camera, very different at poloidally identical locations on the inner limiters in different modules. This made a direct comparison of the different measurements very complicated. In the coming divertor campaign the geometric design of the individual divertor modules will leave much less room for problems of this kind to arise. Apart from that most of the divertor diagnostics will be located within the same divertor module.

6. Summary

The effectiveness of the 10 newly installed control coils has been demonstrated in several important areas. The ability to change the core plasma radius has been verified. Measurements with the poloidal Langmuir probe array showed that in the course of a control coil current ramp the footprints behave as expected from vacuum field calculations. Moreover we have been able to show that the control coils can be used to influence the ratio of perpendicular to parallel transport within an island by nearly a factor 2.

High recycling conditions have been attained at the inboard limiters for $\iota(a) = 5/9$ but there was no indication of detachment. The achieved high recycling conditions in the present very open 'divertor structure' show that we are in a good position to provide a large range of conditions for successful studies of a real island divertor in the upcoming experimental campaign. Excellent data consistency has been achieved during the high density phase of the high recycling discharges between the saturation current I_{sat} measured by the target Langmuir probes and the equivalent values derived from the new absolutely calibrated signal of the 2D H_α CCD camera, using the n_e and T_e values derived by the probes for the calculation of the number of ionisations per photon.

Poloidal as well as toroidal asymmetries caused considerable problems when we tried to relate the measurements of the different edge/target diagnostic signals, since most of the diagnostics were located in different modules or were only taking measurements at the top or the bottom inboard limiter in a particular module. An E_rxB drift might be one possible cause for the observed poloidal asymmetries (e.g., in module 5, H_α) but vacuum field line calculations have also shown that in some modules the asymmetries are most likely caused by toroidally non-symmetrically distributed components like the diamagnetic loop (module 5) or the MINISOX camera (module 3). These problems will partly be avoided in the coming divertor campaign by concentrating most of the edge diagnostics within one divertor module and partly be attacked by specific diagnostics and experiments to investigate the asymmetry problem. Apart from that the new divertor structure can be expected to be at least inherently less prone to such shading effects.

References

[1] J.P. Knauer, G. Kühner et al., in: 12th International Stellarator Workshop, Madison, USA, 1999.
[2] J. Sallander et al., in: 12th International Stellarator Workshop, Madison, USA, 1999.
[3] D. Hildebrandt et al., in: 12th International Stellarator Workshop, Madison, USA, 1999.
[4] Y. Feng et al., in: 12th International Stellarator Workshop, Madison, USA 1999.
[5] K. McCormick et al., Plasma Phys. Contr. Fusion 41 (1999) B285.
[6] K. McCormick et al., these Proceedings.
[7] P. Grigull et al., in: 26th EPS Conference on Fusion and Plasma Physics, Maastricht, 14–18 June 1999, p. 1473.
[8] P. Grigull et al., in: 12th International Stellarator Workshop, Madison, USA, 1999.
[9] P. Grigull et al., these Proceedings.
[10] H.P. Summer, ADAS, JET Report JET-IR(94)06 1994.
[11] Y. Feng et al., Plasma Phys. Contr. Fusion 40 (1998) 371.